Photoacoustic spectroscopy using quantum-cascade lasers

B. A. Paldus, T. G. Spence, and R. N. Zare

Department of Chemistry, Stanford University, Stanford, California 94305-5080

J. Oomens, F. J. M. Harren, and D. H. Parker

Department of Molecular and Laser Physics, University of Nijmegen, Toernooiveld, 6500 GL Nijmegen, The Netherlands

C. Gmachl, F. Cappasso, D. L. Sivco, J. N. Baillargeon, A. L. Hutchinson, and A. Y. Cho

Bell Laboratories, Lucent Technologies, 700 Mountain Avenue, Murray Hill, New Jersey 07974

Received September 18, 1998

Photoacoustic spectra of ammonia and water vapor were recorded by use of a continuous-wave quantum-cascade distributed-feedback (QC-DFB) laser at 8.5 μm with a 16-mW power output. The gases were flowed through a cell that was resonant at 1.6 kHz, and the QC-DFB source was temperature tuned over 35 nm for generation of spectra or was temperature stabilized on an absorption feature peak to permit real-time concentration measurements. A detection limit of 100 parts in 10^9 by volume ammonia at standard temperature and pressure was obtained for a 1-Hz bandwidth in a measurement time of 10 min. © 1999 Optical Society of America

OCIS codes: 000.1570, 140.5960, 120.6200.

Development of sensitive yet robust techniques for detecting trace gases has been of primary importance in applications such as pollution monitoring, biomedical sensing, and atmospheric research. Photoacoustic spectroscopy (PAS), based on the photoacoustic effect, in which acoustic waves result from the absorption of light by a species of interest, has emerged as a potential player in the arena of ultrasensitive detection. PAS makes use of diverse laser sources emitting in the mid infrared[1]: optical parametric oscillators, optical mixers, spin-flip Raman lasers, and high-pressure gas lasers. PAS exploits the high output powers of these sources even though they tend to suffer from one or several of the following drawbacks: complex operation and design, large size and (or) weight, high cost, significant electrical and (or) cooling requirements, substantial linewidths, and a lack of continuous tuning ability.

The recent advent of widely tunable mid-infrared single-mode quantum-cascade distributed-feedback (QC-DFB) lasers[2] capable of emitting tens to hundreds of milliwatts of power and having linewidths of the order of tens of megahertz[3] promises to mitigate many of the aforementioned problems. Quantum-cascade lasers are a new and fundamentally different semiconductor laser source for the mid- and far-infrared regions of the spectrum.[4] These lasers derive their gain from an electronic transition between excited subbands of closely coupled quantum wells. So far, QC lasers with wavelengths from 3.5 to 13 μm (Refs. 5 and 6) have been fabricated by use of the same material system (InGaAs wells and InAlAs barriers) grown by molecular beam epitaxy. In spectroscopic applications QC-DFB lasers can be operated either in pulsed mode at room temperature[7] or in cw mode at cryogenic temperatures.[3] QC-DFB lasers have produced excellent detection sensitivities in both pulsed-mode wavelength modulation spectroscopy (5×10^{-5} noise-equivalent absorbance)[7] and cw-mode rapid-scan direct absorbance spectroscopy (3×10^{-6} noise-equivalent absorbance).[3] The application of cw-mode QC-DFB lasers to PAS of ammonia at 8.5 μm is presented in this Letter.

In this experiment (see the schematic in Fig. 1) a QC-DFB laser was mounted inside a liquid-helium-cooled cryostat (Janis). Its temperature was stabilized to 0.1 °C, and temperature changes were monitored with 0.01 °C precision. For cw operation, current with stabilization (0.1%) was provided by a Kepco power supply. For pulsed operation, current pulses were provided by a Hewlett-Packard supply. The QC-DFB laser was tuned over 35 nm by sweeping of the heat-sink temperature, T_h, from 23 to 88 K, while the laser output power was held constant. Typical QC-DFB heat-sink temperature tuning curves, $\lambda_h(T_h)$, were quadratic and showed a reproducible $\lambda_h(T_h) = 5.65 \times 10^{-6}\ {T_h}^2 - 8.70 \times 10^{-5}\ T_h + 8.487$ dependence. The temperature (T_l) tuning curve of the laser device itself, $\lambda_l(T_l)$, is reliable and fixed and depends on only the waveguide parameters of the laser device. However, T_l can differ from T_h, so $\lambda_h(T_h)$ must be calibrated for each laser cooling system. For real-time ammonia concentration measurements the laser wavelength was fixed to an ammonia feature. In cw operation the laser beam intensity was externally modulated at 1660 Hz with a 50% duty cycle by use of a mechanical chopper.

The resonant photoacoustic cell (PAC), similar to that described in Ref. 8, consisted of an acoustic resonator

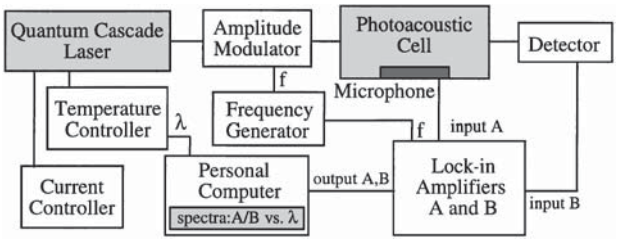

Fig. 1. Block diagram of the photoacoustic apparatus.

0146-9592/99/030178-03$15.00/0

(100 mm long, 8-mm diameter, gold-coated copper inside brass housing) placed between two buffer volumes (50 mm long, 40-mm diameter). The PAC had two tunable air columns at each buffer volume to reduce acoustic signals produced by window heating.[8] The gas inlet was at the resonator center, and gas outlets were at the buffer volumes. Acoustic notch filters were employed at all inlets and outlets[8] for reduction of flow noise and external acoustic interference. Flow rates of 2 L/h were chosen for minimization of flow noise. The weight of the PAC (13 kg) reduced its susceptibility to mechanical vibrations and rendered acoustic shielding unnecessary. The QC-DFB beam entered and exited the acoustic resonator through ZnSe Brewster windows, passing through the PAC once. The QC-DFB beam was focused to a 1-mm waist inside the PAC and detected after the PAC by use of a liquid-nitrogen-cooled HgCdTe detector (Kolmar Technologies) and a lock-in amplifier (SRS510).

A 1-mm^2 electret microphone (Knowles; 22 mV/Pa, 40 $nV/Hz^{1/2}$) was centered in the resonant cell on the antinode of the first longitudinal acoustic mode. The microphone electrical signal was detected by a lock-in amplifier (SRS830), whose signal amplitude and phase were recorded with a 1.0-s integration time constant. In an optimized system the microphone produced a 0.2-$\mu V_{rms}/Hz^{1/2}$ incoherent background signal for pure nitrogen flow (2 L/h) in the PAC. The coherent background (acoustic noise at 1660 Hz, e.g., window-heating effects) was lower than the incoherent noise because of the relatively low laser power (<20 mW). The PA signal was normalized with the intensity measured by the HgCdTe detector.

A gas mixture of ammonia and nitrogen (Praxair; Medipure grade) was prepared in a holding tank. The holding tank was connected through a needle valve and flow regulator to the PAC. Ammonia–nitrogen mixtures ranging from several parts in 10^9 (ppb) to several thousand parts in 10^6 (ppm) were prepared and flowed through the PAC.

Figure 2 illustrates typical spectra. The QC-DFB laser was scanned continuously in wavelength from 8.490 μm (23 K) to 8.525 μm (92 K). The dominant spectral feature at 8.495 μm corresponds to overlapping rovibrational transitions of the $\nu_2 R(10)$ multiplet of ammonia, and the line at 8.514 μm is a single water absorption line. Scans were performed with the gas at standard pressure (1 atm) and temperature (300 K) (STP), so that the ammonia rotational lines were pressure broadened to several gigahertz, producing a composite spectrum. For water vapor, only a single 8-GHz transition was present, in good agreement with HITRAN96 (Ref. 9) for STP. It can be noted that a significant difference exists in the spectra obtained when the QC-DFB laser was temperature tuned slowly (0.5 nm/min) or quickly (5 nm/min). For slow tuning little or no mode instability was observed during the wavelength scan. Hence, the absorption spectra obtained from slow scans reproduce closely their simulated HITRAN96 counterparts. Absorption spectra obtained by use of rapid scans (5 nm/min) show some deviations from simulated spectra. Laser mode instabilities occurred at two wavelengths (8.497 and 8.509 μm) during the entire 35-nm scan. The mode instability could be observed either through laser power fluctuations (≈20%) on the power-calibration detector or as transverse-mode coupling changes on a ZnSe Fabry–Perot etalon (5 cm long, 3-GHz free spectral range), resulting in 1–2-nm spectral shifts [as shown in the ammonia feature in Fig. 2(a) based on simulated spectra]. We attribute these instabilities to residual reflections from the cleaved facets of the laser, which were not antireflection coated. However, this mode instability could be almost entirely eliminated by adjustment of the laser supply current to ensure laser mode structure and a constant power level or by use of software calibration for extrapolation of the spectral feature after the mode-instability region was excluded from the scan data set.

As shown in Fig. 2(b), the water line that is present in all ammonia mixture spectra arises from impurity moisture in the ammonia source itself. The water absorption feature is a single transition, whereas the ammonia feature contains many unresolved transitions. Therefore, the moisture concentration could be correlated with the integrated line intensity or with peak absorbance. The ammonia concentration, however, corresponded only to the integrated line intensity, so scanning over the spectral feature was necessary to provide an accurate measure of ammonia concentration. Single-wavelength dynamic measurements required additional calibration for correct estimation of concentration.

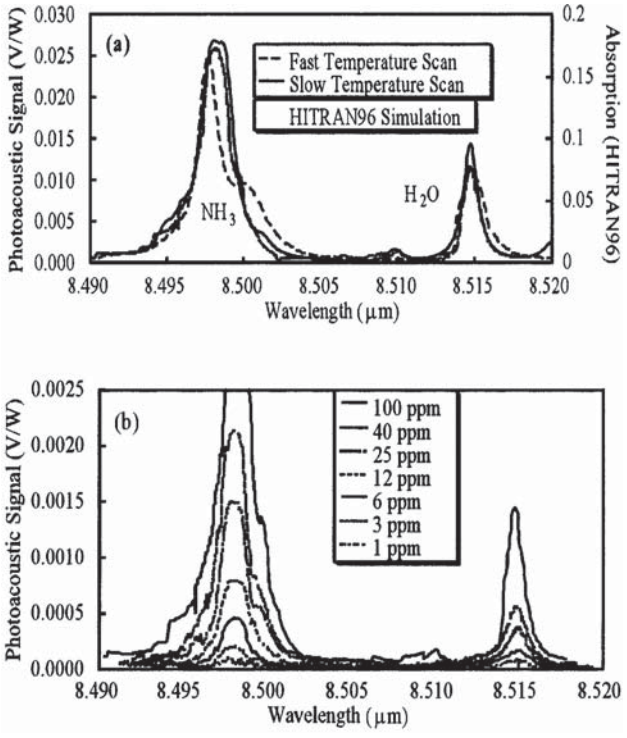

Fig. 2. Photoacoustic spectra of NH_3 and H_2O diluted with nitrogen at STP: (a) slow (0.5-nm/min) and fast (5-nm/min) temperature tuning spectra compared with HITRAN96 simulations (50-ppm ammonia mixture), (b) slow-scan spectra corresponding to various mixture dilutions. All lines are pressure broadened to several gigahertz.

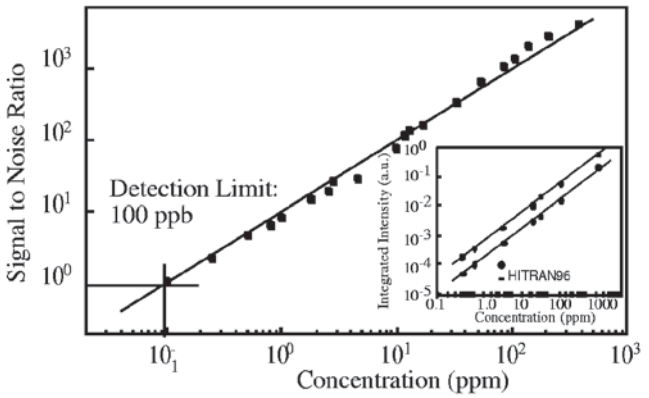

Fig. 3. Signal-to-noise ratio of NH_3 peak absorption for averaged fast scans (5 nm/min). The inset shows integrated intensity versus concentration (units differ for HITRAN96 simulations and PAS owing to nonabsolute concentration calibration).

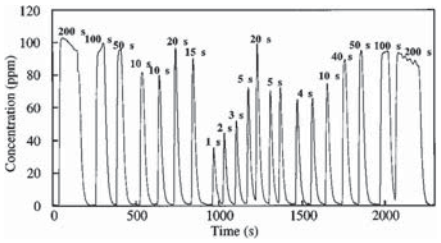

Fig. 4. Real-time NH_3 concentration monitoring by use of the 8.498-μm peak absorbance for a 100-ppm NH_3–N_2 mixture injected into a N_2 stream. The mixture bolus injection time is indicated for each cycle. The cell was operated at STP (2-L/h flow rate). The gas mixture was interrupted with a mechanical valve.

Figure 3 illustrates the dependence of the measured signal-to-noise ratio of the ammonia feature peak on ammonia partial pressure for an optically optimized system in which the optics maximize the light intensity reaching the PAC while minimizing the PAC background noise by controlling the beam shape. Spectra were obtained for ammonia concentrations ranging from 2200 ppm to 100 ppb by volume. The sensitivity limit for the NH_3 spectral feature is ~220 ppb (2×10^{-5} noise-equivalent absorbance) for rapid temperature sweeps (5 nm/min) but can be reduced to 100 ppb (8×10^{-6} noise-equivalent absorbance) either by slow (<1 nm/min) temperature sweeps over a reduced portion of the spectrum or by averaging continuously over eight wavelength points in the fast-scan spectra. The measurement time for the 100-ppb scans was 10 min. The sensitivity obtained is comparable with that achieved by the rapid-scan technique,[3] although scan times are longer for PAS. Absolute calibration between HITRAN96 and the PAS signal intensity (1% absolute accuracy for the gas-handling system) was not performed, and so the inset of Fig. 3 has arbitrary units. Real-time ammonia monitoring results are shown in Fig. 4 for a 100-ppm ammonia–nitrogen mixture at STP, a QC-DFB 0.5-A current, and 52 K T_h (i.e., ammonia peak absorbance at 8.498 μm). The gas-system response time was 15 s. The minimum detectable gas turn-on time was limited by gas-system mechanics to 1 s. The minimum detectable concentration was 250 ppb for 1 s in a 2-L/h flow. Ammonia absorption–desorption in both the PAC and the gas-delivery system produced peak height variation for identical mixture bolus injection times. The integrated areas remained constant for identical injection times, despite the peak height variation.

The sensitivity achieved here can be related to previous PAS work.[9] To a good approximation, the PA signal is proportional to laser output power and to the partial pressure and the absorption coefficient of the sample gas. The previously obtained record PAS detection limit for C_2H_4 for an intracavity 100-W CO_2 laser[9] and an effective absorption coefficient of 23.7 atm^{-1} cm^{-1} was 0.006 ppb. For the current system the QC-DFB power was 16 mW and the absorption coefficient was 14.8 atm^{-1} cm^{-1}. The predicted sensitivity is 60 ppb, which corresponds to the 100-ppb sensitivity that was achieved. The QC-DFB laser was also pulsed with 100-ns-long current pulses at a 1660-Hz repetition rate. The duty cycle (1.7×10^{-4} compared with 0.5) of the laser beam intensity reduced PAS sensitivity, but with proper redesign of the system PAS using pulsed QC-DFB lasers at room temperature can be achieved.

The work at Stanford University was supported by the Air Force Office of Scientific Research (contract F49620-98-1-0040). J. Oomens, F. J. M. Harren, and D. H. Parker thank the Technology Foundation STW, the Applied Science Division of NWO, and the Technology Program of the Ministry of Economic Affairs. The work at Bell Laboratories was supported in part by the Defense Advanced Research Projects Agency/U.S. Army Research Office (contract DAAH04-96-C-0026).

References

1. M. Sigrist, *Air Monitoring by Spectroscopic Techniques* (Wiley, New York, 1994), pp. 163–227.
2. F. Capasso, J. Faist, C. Sirtori, and A. Y. Cho, Solid State Commun. **102,** 231 (1997).
3. S. W. Sharpe, J. F. Kelly, J. S. Hartman, C. Gmachl, F. Capasso, D. L. Sivco, J. N. Baillargeon, and A. Y. Cho, Opt. Lett. **23,** 1396 (1998).
4. C. Gmachl, F. Capasso, J. Faist, A. Hutchinson, A. Tredicucci, D. Sivco, J. Baillargeon, S. Chu, and A. Cho, Appl. Phys. Lett. **72,** 1430 (1998).
5. J. Faist, F. Capasso, D. L. Sivco, A. L. Hutchinson, M. Beck, S. N. G. Chu, and A. Y. Cho, Appl. Phys. Lett. **72,** 680 (1998).
6. C. Gmachl, F. Capasso, A. Tredicucci, D. L. Sivco, A. Hutchinson, and A. Cho, Electron. Lett. **34,** 1103 (1998).
7. K. Namjou, S. Cai, E. A. Whittaker, J. Faist, C. Gmachl, F. Capasso, D. L. Sivco, and A. Y. Cho, Opt. Lett. **23,** 219 (1998).
8. F. G. C. Bijnen, J. Reuss, and F. J. M. Harren, Rev. Sci. Instrum. **67,** 2914 (1996).
9. http://www.hitran.com.
10. F. J. M. Harren, F. G. C. Bijnen, J. Reuss, L. A. C. J. Voesenek, and C. N. P. M. Blom, Appl. Phys. B **50,** 137 (1990).